Nanostructured gold films as broadband terahertz antireflection coatings

Andreas Thoman, Andreas Kern, Hanspeter Helm, and Markus Walther
Freiburg Materials Research Center, University of Freiburg, Stefan-Meier-Strasse 21, D-79104 Freiburg, Germany
(Received 22 February 2008; revised manuscript received 2 April 2008; published 6 May 2008)

The potential of nanometer-thick, randomly nanostructured gold films as broadband wave impedance-matching coatings for nondispersive substrates in the terahertz frequency range is demonstrated. Based on a wave impedance approach and the specific non-Drude conductivity of our films, we model the reflectivity at the coated interface between silicon and air and show that nanostructured films offer a considerably better broadband performance than conventional bulk metallic layers. The predictions from the theoretical model are verified in experimental studies of different gold nanostructures investigated by terahertz time-domain spectroscopy in the frequency range of 0.2–2.2 THz. An extension of a previously developed subgridding scheme for the finite-difference time-domain method allows us to simulate terahertz-pulse propagation through uncoated and coated samples and to follow attenuation and reshaping of the internally reflected pulse when the film thickness is varied with subnanometer precision.

DOI: 10.1103/PhysRevB.77.195405 PACS number(s): 78.20.−e, 07.57.Kp, 78.66.−w

I. INTRODUCTION

Over the past decades, there have been tremendous advances in the generation, manipulation, and detection of terahertz radiation. All these new technologies have inspired exciting new applications for terahertz sensing and imaging. Their technical implementation requires sources, detectors, and optical components such as beam splitters, dispersive optical elements and substrates, or windows transparent in the far-infrared region. Typically, these components cause reflections due to the refractive index mismatch at interfaces giving rise to unwanted Fabry–Pérot behavior. In such cases, antireflection coatings that operate at terahertz frequencies would be highly advantageous to minimize étalon reflections.

Due to their small bandwidth, standard dielectric quarter-wave antireflection coatings are not suitable for experiments with multiple wavelengths or broadband terahertz pulses. Therefore, alternative concepts for effective reflex suppression have to be employed. Recently, ultrathin metallic films were demonstrated to work as efficient impedance-matching layers in the terahertz and midinfrared frequency ranges, showing broadband performance.[1,2] In this experiment, chromium films were specifically chosen due to their good adhesion properties and long-term stability. Chromium forms homogeneous layers already at very low evaporated film thicknesses, which provides good control over the film properties during film production. Other metals such as gold show highly inhomogeneous film growth in the required thickness range, exhibiting a crossover between an insulating and a metallic phase via a percolation transition.[3–5] Therefore, such films were thought not to be suitable as impedance-matching layers mainly due to their uncontrollable nanostructure.

In this paper, we show in theory and experiment that randomly nanostructured gold films represent antireflection coatings with a significantly better broadband performance than homogeneous metal films at least in the terahertz frequency range. Owing to their characteristic non-Drude behavior, our films show a nearly frequency-independent sheet conductivity, which allows to perfectly match the impedance over an extended frequency range. This is usually not possible for bulk metallic films that typically show frequency-dependent Drude behavior. We demonstrate that with our nanostructured gold films, the internal reflection of a broadband terahertz pulse (spectral bandwidth of 0–3 THz) at a silicon-air interface can be suppressed to $<1\%$ of its initial field amplitude without coating compared to $>5\%$, which would be the best suppression achievable with bulk gold layers. For our experimental investigations, we utilized two different film preparation methods based on a chemical deposition technique and on sputtering gold clusters onto the substrate, respectively. Both techniques allow us to produce well adherent, stable films and provide good reproducibility and sufficient control over the films' sheet resistance.

The organization of this paper is as follows. In Sec. II, we describe the film preparation methods and briefly introduce the experimental setup. In Sec. III, the theory for field transmission through thin metallic layers on thick substrates is reviewed and the requirements for broadband impedance matching are discussed. Furthermore, we introduce the Drude–Smith model, which provides a very good approximation for the complex conductivity of our nanostructured gold films. In Sec. IV, we show the experimental results for various films including fits of the Drude–Smith model to our measured film conductivity. A simulation using the finite-difference time-domain method of the terahertz-pulse transmission through bulk and nanostructured gold films is presented in Sec. V. This simulation allows us to quantify the best suppression of the internal reflection achievable by both film types. Finally, a conclusion is given in Sec. VI.

II. EXPERIMENTAL METHODS

A. Film fabrication and characterization

Two different thin film preparation methods were used to coat 520 μm thick Si(100) substrates with nanometer-thick inhomogeneously nanostructured gold layers. Both techniques produce gold films with different characteristic nanoscopic morphologies.

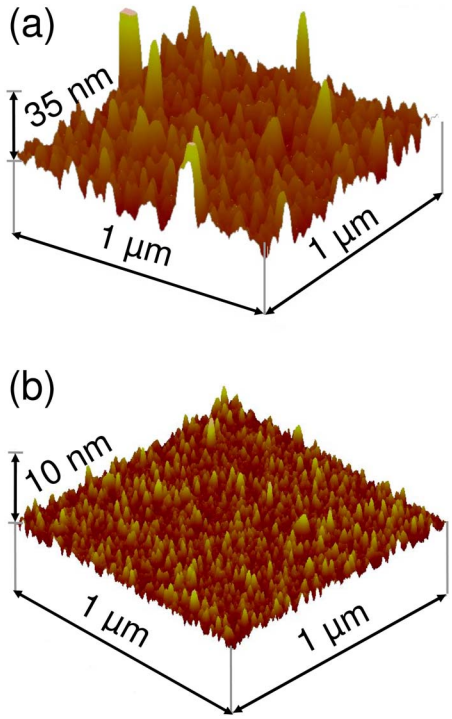

FIG. 1. (Color online) AFM images of (a) a chemically deposited gold film and of (b) a gold film produced by sputtering gold clusters onto the silicon substrate.

For the first set of samples, a chemical (electroless) deposition technique[6] was applied to deposit gold onto the carefully cleaned and subsequently hydrogen terminated silicon surface. Following the protocol reported by Miyake *et al.*,[6] deposition was performed at an elevated temperature (60 °C) by dropping a plating solution consisting of $0.015M$ $NaAuCl_4$+$0.15M$ Na_2SO_3+$0.05M$ $Na_2S_2O_3$ +$0.05M$ NH_4Cl together with 2% HF onto the silicon surface. In this environment, the silicon is oxidized, forming a fluoride complex, and the released electrons reduce the gold ions, which then form neutral gold. The effective film thickness can be controlled during this process by the deposition time. Depending on the required thickness, after 10–200 s, the deposition was terminated by rinsing the sample with deionized water. The atomic force microscope (AFM) image of a selected film in Fig. 1(a) shows the formation of individual gold islands with about 20–30 nm average diameter with occasional accumulations of larger gold clusters. The partially overlapping islands form an inhomogeneous network consisting of gold and void regions. AFM images of thicker films show that with increasing the effective film thickness, larger gold accumulations occur. However, the fine colloidal structure in between these clusters is maintained.

Alternatively, thin films have been produced by energetic cluster impact (ECI) deposition.[7,8] In this technique, charged gold clusters are accelerated by an electric field onto the clean silicon substrate. The gold clusters are produced by a magnetron sputter discharge within a gas aggregation source. Gold atoms are sputtered from the discharge into a mixture of helium and argon with a pressure of about 0.5 mbar, where clusters are formed. A large part of the clusters is ionized and can be accelerated by an electric field and directed onto the silicon target. The impact energy of the deposited clusters can be controlled by the substrate potential. For our samples, a moderate impact energy of about 2 keV was chosen. The deposited film thickness is controlled by the time the target was exposed to the cluster beam. An AFM image of a gold film produced by ECI deposition is shown in Fig. 1(b). Again, the film consists of individual partially overlapping gold islands. Their size distribution is much more homogeneous than that for the films produced by the chemical deposition technique with an average diameter on the order of 10 nm.

Due to the reaction with the Si surface, the chemically deposited gold island films showed better adhesion properties than comparable films produced by vacuum evaporation[3] or the cluster deposition technique, which showed comparable stability against mechanical treatment. However, the optical properties of all the films, such as their terahertz transmission and conductivity, appeared to be stable over several months.

B. Terahertz time-domain spectroscopy

A standard terahertz time-domain spectrometer (TDS) in transmission geometry[9] was used to characterize the samples in the frequency range between 200 GHz and 2.2 THz. Briefly, two photoconductive dipole antennas driven by femtosecond pulses from a mode-locked Ti:sapphire oscillator (12 fs, 800 nm, 76 MHz) are used to generate and detect the terahertz transient. The generated terahertz pulses radiate into free space and are guided by two off-axis paraboloidal mirrors, which produce a frequency-independent focus with about ~5 mm diameter at the sample position. Another pair of paraboloidal mirrors focuses the pulses onto the detector antenna. By a variable optical delay, the terahertz pulses generated at the emitter can be continuously delayed with respect to the gated detector, which allows to temporally scan their electric field. In a typical terahertz TDS measurement, the time-dependent electric field of the terahertz pulse transmitted through a sample is determined and by a subsequent Fourier transformation, the corresponding complex frequency spectrum is determined. All measurements were performed at room temperature and at ambient pressure in a nitrogen-purged environment to avoid water vapor absorption.[10]

III. THEORETICAL BACKGROUND

A. Fresnel equations for a thin conducting film on a thick substrate

At the interface between two media with different refractive indices n_1 and n_2, reflections appear. Similar reflections occur when an electric signal propagates from one transmission line with impedance Z_1 to a second one with Z_2. Therefore, a convenient method to describe wave propagation in inhomogeneous optical media is to represent the system by an equivalent transmission line circuit with characteristic

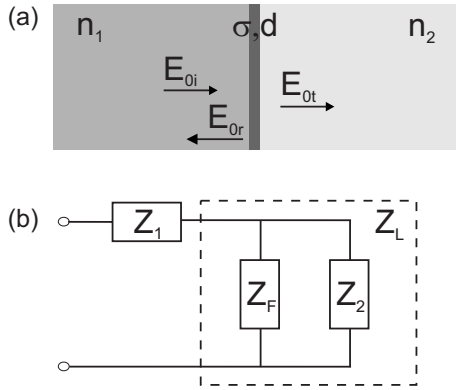

FIG. 2. (a) Two dielectric media with refractive indices n_1 and n_2 separated by a thin conducting film with conductivity σ and thickness d. E_{0i} denotes the incident electric field, E_{0r} denotes the reflected, and E_{0t} denotes the transmitted fields. (b) Wave propagation in the optical system can be represented by signal propagation in an equivalent transmission line circuit with the impedances Z_1, Z_2 and the film impedance Z_F. Z_F and Z_2 contribute to the combined load impedance Z_L.

impedances. The corresponding wave impedance of an electromagnetic wave propagating in a medium is given by the ratio of the tangential components of the electric and magnetic fields:[11]

$$Z = \frac{E_t}{H_t} = \frac{Z_0}{n}, \tag{1}$$

where $Z_0 = \sqrt{\mu_0/\epsilon_0} = 377\ \Omega$ is the impedance of free space, $n = \sqrt{\epsilon}$ is the complex refractive index, and ϵ is the complex permittivity of the medium.

In a thin conducting film with complex conductivity σ, an incident, transverse electric field E induces a current density $j = E\sigma$. If the thickness d of the conducting layer is much smaller than the skin depth δ, j can be assumed to be uniform throughout the film, corresponding to a surface current $J = jd$. If the film separates two media, as sketched in Fig. 2(a), the boundary conditions require that the tangential components of E are continuous across the film, and that the components of H are discontinuous by the surface current.[12] Therefore, in the limit of a very thin film ($d \ll \delta$), its impedance is given by[13]

$$Z_F = \frac{E}{H_1 - H_2} \approx \frac{E}{J} = \frac{1}{\sigma d}, \tag{2}$$

where H_1 and H_2 are the magnetic fields at the two sides of the film.

In the equivalent circuit, a thin conducting layer separating two media corresponds to an additional impedance shunting the line, as illustrated in Fig. 2(b). In this case, the surface current in the film corresponds to a current through the shunting impedance Z_F parallel to Z_2. Both impedances can be combined to the load impedance Z_L, which is then given by

$$\frac{1}{Z_L} = \frac{1}{Z_2} + \frac{1}{Z_F}. \tag{3}$$

At the interface between the source and the load, a time-dependent field gets partially reflected with the amplitude coefficients of reflection and transmission:[13]

$$r = \frac{Z_L - Z_1}{Z_L + Z_1} \quad \text{and} \quad t = \frac{2Z_L}{Z_L + Z_1}. \tag{4}$$

Replacing Z_L in Eq. (4) by the expression in Eq. (3) and using the individual impedances from Eqs. (1) and (2) yields

$$r = \frac{n_1 - n_2 - Z_0\sigma d}{n_1 + n_2 + Z_0\sigma d} \tag{5}$$

and

$$t = \frac{2n_1}{n_1 + n_2 + Z_0\sigma d}. \tag{6}$$

Note that if the thickness d (or the conductivity σ) of the film approaches zero, we get the well known Fresnel equations for the reflection and transmission coefficients at the interface between two dielectric media,[14]

$$r_0 = \frac{E_{0r}}{E_{0i}} = \frac{n_1 - n_2}{n_1 + n_2}, \quad t_0 = \frac{E_{0t}}{E_{0i}} = \frac{2n_1}{n_1 + n_2}. \tag{7}$$

B. Impedance matching

According to Eq. (4), the reflection can significantly be reduced by decreasing the impedance mismatch across the interface. In order to fully suppress the reflection of a signal back into the source, the load impedance must be exactly matched to the source impedance ($Z_L = Z_1$), which is, in general, a complex valued function of frequency. Therefore, generally, both the real and imaginary components of the impedances have to be matched, which complicates the task. Since in many optical applications, however, window materials and substrates are chosen due to their low attenuation, absorption in these media can usually be neglected and their wave impedances are real valued. Silicon, for example, is a popular window material in the far infrared due to its very low absorption in this wavelength region.

Impedance matching between two media separated by a thin conducting film, as in Fig. 2(a), can be achieved by choosing the film impedance Z_F so that the combined load impedance Z_L is equal to Z_1. However, since in a parallel circuit Z_L is always smaller than either of its individual components Z_F and Z_2, impedance matching can only be achieved for $Z_2 > Z_1$. Thus, in our system, impedance matching by a thin conducting layer can only be achieved at the transition from the optically thick (silicon) to the optically thin medium (air) and not vice versa. Note that this is a general limitation of wave impedance-matching layers for optical applications. To achieve zero reflectance at the opposite interface (air-silicon), one needs to increase the combined load impedance, which is possible in a transmission line circuit by adding an additional impedance in series to Z_2, but this cannot be achieved in the optical equivalent by a conductive coating.

To eliminate the reflection at the silicon-gold-air interface, the numerator in Eq. (5) has to vanish, and we have to fulfill the condition

$$n_{\mathrm{Si}} - n_{\mathrm{air}} = Z_0 \sigma d, \tag{8}$$

with both refractive indices being real and nearly constant over the frequency range covered by our experiment ($n_{\mathrm{air}}=1.00$ and $n_{\mathrm{Si}}=3.42$). Since Z_0 and d are constant real numbers, fulfilling Eq. (8) requires that also the complex conductivity $\sigma=\sigma_1+i\sigma_2$ be real and constant over the entire frequency range. Therefore, in order to perfectly eliminate all back reflections at the interface through impedance matching, we need a conducting layer with

$$\sigma_1 = \frac{n_{\mathrm{Si}} - n_{\mathrm{air}}}{Z_0 d} = \mathrm{const}, \quad \sigma_2 = 0. \tag{9}$$

As we will show below, this is a requirement that conventional bulk metallic layers do not fulfill. Although it has been argued that for most metals at terahertz frequencies we are in a regime where the conductivity is only weakly frequency dependent with negligible imaginary component,[1] in practice, the applicability of conventional bulk metallic antireflection coatings is limited to cases where residual reflections can be tolerated.

On the other hand, nanostructured metallic layers can show conductivities that deviate strongly from those of bulk metal films, which usually follow the standard Drude model,[3] due to their discontinuous film morphology. As we will show below, such films may exhibit the desired conductivity behavior in Eq. (9) and enable a nearly perfect broadband impedance matching.

C. Measuring the film conductivity

The complex conductivity of our films has been determined by measuring the time-dependent electric field of a broadband terahertz pulse transmitted through the thin film sample, $E_{\mathrm{substrate+film}}(t)$, as well as through the uncoated substrate, $E_{\mathrm{substrate}}(t)$, as reference (Fig. 3). Fourier transformation of the main pulses [solid lines in Fig. 3(b)] then yields the complex, frequency-dependent terahertz spectra, $E_{\mathrm{substrate+film}}(\omega)$ and $E_{\mathrm{substrate}}(\omega)$. Their ratio corresponds to the ratio of the transmission coefficients in Eqs. (6) and (7) and yields[3,15]

$$\frac{E_{\mathrm{substrate+film}}(\omega)}{E_{\mathrm{substrate}}(\omega)} = \frac{t}{t_0} = \frac{1+n_{\mathrm{Si}}}{1+n_{\mathrm{Si}}+Z_0\sigma(\omega)d}, \tag{10}$$

where the refractive index of air has been inserted and $n_{\mathrm{Si}}=3.42$ is the refractive index of the silicon substrate, which has been determined in a separate measurement. This expression first introduced by Tinkham[16] is valid if the films are much thinner than the wavelength and the skin depth, which are both fulfilled for our films. Equation (10) directly allows us to determine the complex conductivity from the measured spectra.

By monitoring the second pulse, which corresponds to the first internal reflection in the substrate (dashed section in Fig. 3), we can investigate the antireflection behavior of our gold film samples.

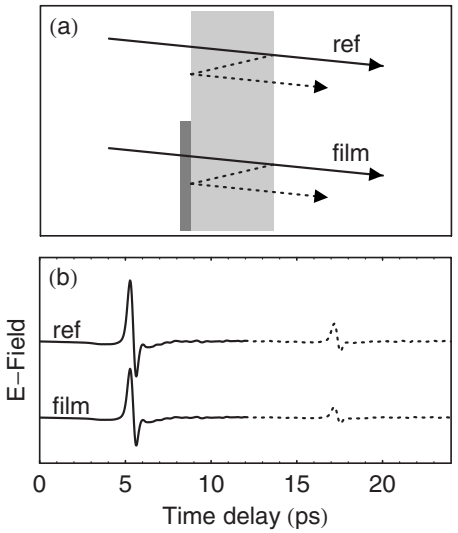

FIG. 3. (a) Illustration of terahertz-pulse propagation through the uncoated and coated silicon substrate, as measured in our experiment. The first internal reflection in the silicon substrate is indicated by the dashed line. The corresponding terahertz wave forms recorded at the detector are shown in (b). Approximately 12 ps after the main pulse, a second, weaker pulse appears, which corresponds to the internal reflection.

D. Drude and Drude–Smith models

The frequency dependence of the complex conductivity of homogeneous metals can be described by the Drude model:

$$\sigma(\omega) = \frac{\epsilon_0 \omega_p^2 \tau}{1 - i\omega\tau}, \tag{11}$$

where ω_p is the plasma frequency and τ is the scattering relaxation time. The corresponding behavior of the real and imaginary parts of σ for bulk gold is shown in Fig. 4(a) assuming literature values from Ref. 17 ($\tau=24.5$ fs, $\omega_p/2\pi=2175$ THz). The condition required for perfect impedance matching in Eq. (9) is only approximately fulfilled for very low frequencies in the so-called Hagen–Rubens regime,[13] where $\omega\tau \ll 1$. Already at a frequency of 1 THz, σ_2 is about 20% of the σ_1 value and, therefore, no longer negligible. Also, the real part of the conductivity σ_1 starts to show a considerable frequency dependence.

Classically, the dielectric properties of composite systems have been modeled by effective medium theories (EMTs), which treat the medium as a composite of two materials with individual dielectric properties, which in our case are a Drude metal and an insulator. Mainly two EMT approaches have been widely adopted, the Maxwell–Garnett[18] and the Bruggeman EMT,[19] which are capable of modeling dilute composite materials and systems that show a distinct insulator-to-metal transition, respectively.[3] For semicontinuous gold films, however, EMT proved to be invalid close to the transition[3,4,20] since effects originating from the intercluster capacitance, which are not included in the theory, increasingly become important as the average cluster separation approaches zero. Also, in EMT, the binary mixture of particles is not considered in contact with an interface, and therefore,

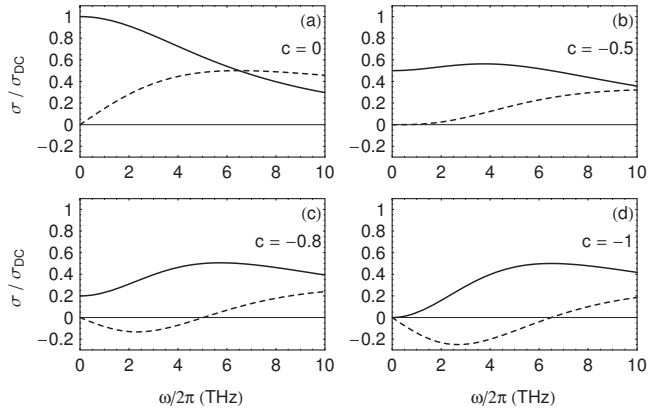

FIG. 4. (a) Real (solid line) and imaginary parts (dashed line) of the complex conductivity of bulk gold following the Drude model. (b)–(d) show the conductivity according to the Drude–Smith model in Eq. (13) for different nonzero values of c.

interaction with the substrate is usually disregarded. A scaling approach derived from percolation theory[21] yielded a much better agreement at all wavelengths from the near to the far IR (Ref. 4) but requires the introduction of specific scaling functions that depend on the film's microgeometry. An alternative model that has been successfully applied to various conducting, nanostructured systems that show deviations of the terahertz conductivity from standard Drude behavior[3,15,22–25] is based on a generalized Drude formalism developed by Smith.[26]

Within the Drude–Smith model, the complex conductivity is given by

$$\sigma(\omega) = \frac{\epsilon_0 \omega_p^2 \tau}{1 - i\omega\tau}\left[1 + \sum_j \frac{c_j}{(1 - i\omega\tau)^j}\right], \tag{12}$$

where c_j is a parameter describing the persistence of the charge carrier's initial velocity after j scattering events. In practice, only the first scattering term is taken into account such that $c_j=0$ for $j>1$ and $c_1 \equiv c$. Neglecting higher order scattering terms corresponds to a transition from ballistic (first collision) to diffuse (subsequent collisions) carrier propagation.[26] In this case, c can range from $c=0$ (isotropic scattering as assumed in the Drude model) to $c=-1$ (full carrier back scattering) and Eq. (12) simplifies to

$$\sigma(\omega) = \frac{\epsilon_0 \omega_p^2 \tau}{1 - i\omega\tau}\left[1 + \frac{c}{(1 - i\omega\tau)}\right]. \tag{13}$$

Varying parameter c in Eq. (13) affects the real and imaginary components of the conductivity, as illustrated in Fig. 4. For $c=0$ corresponding to isotropic scattering of the carriers, we obtain a normal Drude behavior. With decreasing c, σ_1 gets progressively suppressed at low frequencies. For $c=-1$, the real conductivity σ_1 is completely suppressed at zero frequency and the material becomes an insulator ($\sigma_{dc}=0$). The impeded real part of the conductivity is associated with a change in slope of the imaginary part. For $c<-0.5$, the imaginary conductivity σ_2 becomes negative at low frequencies, which can be understood as a capacitive response of the electrons to the external field, whereas for $c>-0.5$, the response is mainly inductive. In semicontinuous gold films, the crossover between these two cases has been observed at the metal-to-insulator percolation transition[3] and was interpreted as the transition between a situation where the charge carriers are mainly localized within individual gold islands in the insulating phase and free carrier conduction in the metallic phase. For a situation with the c parameter close to −0.5 [Fig. 4(b)], we obtain a nearly constant σ_1 and a σ_2 very close to zero over a broad frequency range extending from 0 to about 3 THz. As discussed above, these are exactly the conditions required for broadband impedance matching at the interface between transparent nondispersive media, such as silicon and air. As we will show, the Drude–Smith model yields very reasonable fits to our conductivity data. It therefore provides a simple analytical expression for the complex conductivity of our films, which will be used in the following to model the film reflectivity and as input for our numerical simulations.

E. Modeling the film reflectivity

To demonstrate the effect of the film thickness and conductivity on its reflectivity at the silicon-air interface, we calculated the frequency-dependent reflection coefficient r according to Eq. (5). For the calculation, we modeled the conductivity of a bulk gold film with the standard Drude expression according to Eq. (11) and of a nanostructured gold layer with a Drude–Smith conductivity, Eq. (13), with $c=-0.55$. In Fig. 5, we plot the absolute value of r as a function of the film thickness d and frequency $\omega/2\pi$ for both coatings. In both cases, we observe a minimum of the reflectivity at zero frequency for an optimal film thickness d_{opt}. However, whereas the reflectivity progressively rises with increasing frequency for the Drude film, the reflection coefficient stays close to zero over a broad frequency range for the coating with Drude–Smith conductivity. This comparison demonstrates the potentially superior performance of nanostructured conducting layers as broadband antireflection coatings in the terahertz regime compared to that of conventional bulk metallic layers.

IV. EXPERIMENTAL RESULTS AND DISCUSSION

In the following, we will present experimental investigations of our fabricated nanostructured gold films by transmission terahertz TDS.

A. Chemically deposited films

As described in Sec. III C, the frequency-dependent conductivity could be determined from the terahertz transmission spectra provided that the film thicknesses are sufficiently well known. However, due to the inhomogeneous film structure, the chemically grown gold films do not exhibit a well-defined thickness. Therefore, it is more appropriate to determine the films' sheet conductance σd, which can be directly inferred from Eq. (10) without the knowledge of d.

Figure 6 shows the real and imaginary parts of the sheet conductance for three selected chemically grown films corresponding to a very thin film with a high film impedance

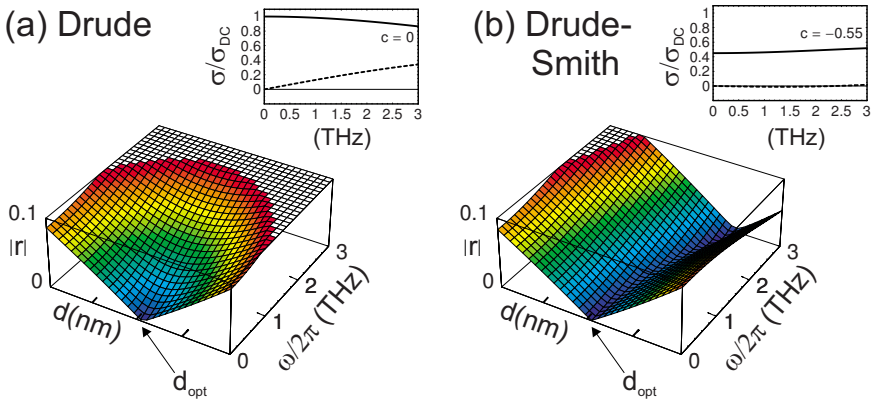

FIG. 5. (Color online) Calculated absolute value of the reflectivity at the silicon-air interface coated with a gold layer following (a) Drude and (b) Drude–Smith conductivity as a function of the film thickness and frequency. The insets show the corresponding conductivity behavior. The plateau indicates an absolute reflection coefficient $|r|$ already greater than 0.1. For realistic values of the conductivity of thin nanostructured gold films, the optimal film thickness d_{opt} is on the order of 10 nm.

(film 1), a gold film of intermediate thickness and impedance (film 2), and a relatively thick gold film with a correspondingly low impedance (film 3). From AFM profiles, we could estimate only a very approximate thickness distribution ranging from 5 to 15 nm for film 1, from 10 to 25 nm for film 2, and from 15 to 30 nm for film 3.

All of the films show a nearly constant real part of the conductivity over the investigated frequency range with the imaginary part very close to zero. This observed conductivity behavior cannot be modeled by a standard Drude model. In agreement with a previous study on nanostructured gold films, we found that the Drude–Smith approach provides very reasonable fits to our measured sheet conductances. The best fits of the Drude–Smith formalism according to Eq. (13) to the measured $\sigma_1 d$ and $\sigma_2 d$ are plotted for all of the films in Fig. 6.

The characteristic deviation from the standard Drude behavior is illustrated in Fig. 7 for film 2. The dashed line shows a fit of the Drude model to the data points, which obviously fails to reproduce the observed behavior. The Drude–Smith model (solid line), on the other hand, provides a very good fit. For this particular film, we obtain the best-fit parameters $\tau = 18$ fs and $\omega_p/2\pi = 0.0474/\sqrt{d}$ and $c = -0.55$, which are in reasonable agreement with values reported for nanometer-thick, discontinuous gold films near the metal-to-insulator percolation transition.[3] Note that the c parameter is exactly in the region where we expect the best impedance matching due to the nearly constant σ_1 and the vanishing σ_2, as discussed in the previous section. Thus, we expect a considerable suppression of the internal reflection for the proper film thickness (or sheet conductance, respectively).

In Fig. 8, the electric field of the terahertz pulses is plotted after transmission through the different gold film samples together with a terahertz pulse transmitted through the uncoated substrate as reference. With increasing the film thickness, the amplitude of the main pulse decreases as a consequence of rising absorption in the gold film and increasing reflection losses at the air-gold-silicon interface. Approximately 12 ps after the main pulse, a second, weaker pulse appears, which corresponds to the first internal reflection in the silicon substrate (see Fig. 3). Coating the Si surface with the thin films affects the reflex in the following way: The thin layer (film 1) causes a slight decrease in the amplitude of the internal reflection, whereas film 2 leads to a complete suppression. We find that within the uncertainty of our measure-

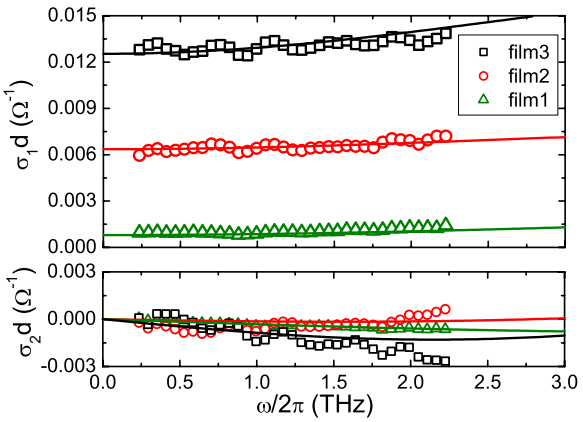

FIG. 6. (Color online) Terahertz sheet conductivity spectra of chemically grown gold films together with Drude–Smith fits (solid lines).

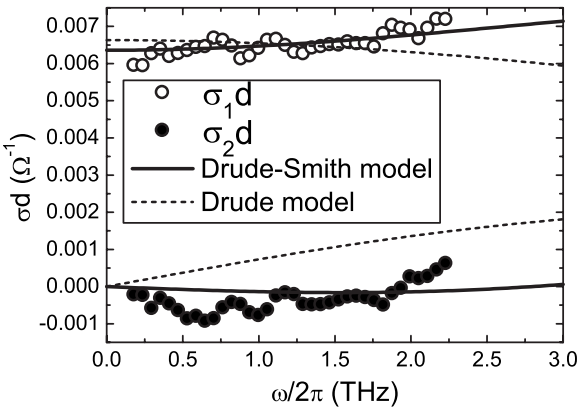

FIG. 7. Measured sheet conductivity spectrum of film 2. The curves represent fits by the Drude (dashed line) and the Drude–Smith model (solid line).

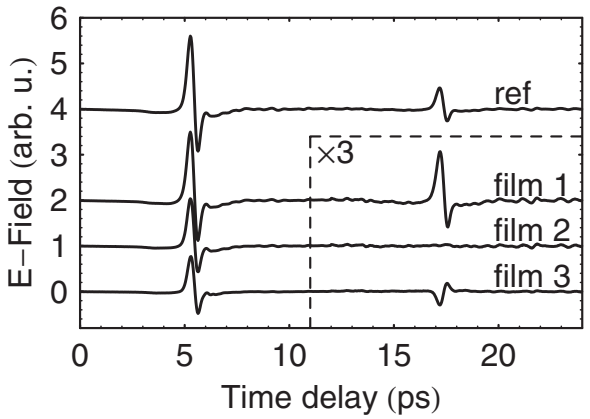

FIG. 8. Terahertz wave forms after transmission through an uncoated Si substrate (ref) and through samples coated with a chemically deposited gold nanostructure (films 1–3). In each time trace, the pulse at later times is due to the internal reflection within the substrate, as indicated in Fig. 3. Film 2 totally suppresses the internal reflection by perfect broadband impedance matching.

ment, for this particular film, no residual reflected pulse was detected, indicating that the conditions stated in Eq. (9) are fulfilled within the bandwidth of our experiment. In this case, still 64% of the initial electric field amplitude of the main pulse is transmitted through the gold layer compared to the reference scan through the uncoated substrate. For film 3, we observe a reversal of the reflected pulse corresponding to a phase shift of π, which is characteristic for a reflection at an interface to an optically denser medium. Here, the impedance of air has been overcompensated by the gold film so that the field incident from the silicon side experiences a medium with a lower effective impedance.

B. Gold cluster films

Since the gold cluster films on silicon substrates produced by the ECI technique show a much more homogeneous surface coverage than the chemically deposited coatings (Fig. 1), an effective film thickness could be specified for all samples, which allows us to directly determine the complex

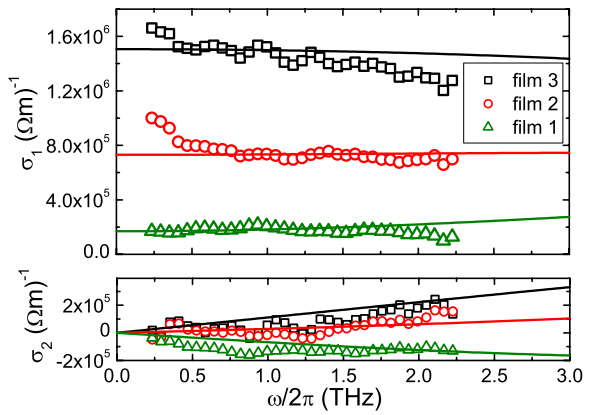

FIG. 9. (Color online) Terahertz conductivity spectra of three gold cluster films with different film thickness (films 1–3). The solid lines are fits according to the Drude–Smith model.

conductivity. The real and imaginary parts of the measured complex conductivity of three films (films 1–3) with d=5.5, 9, and 10.5 ± 1 nm are plotted in Fig. 9. Again, the Drude–Smith model simultaneously provides adequate fits (solid lines) to our measured $\sigma_1(\omega)$ and $\sigma_2(\omega)$, with a given set of fit parameters for each film.

In contrast to the chemically grown films, the best-fit c parameters vary from $c=-0.85$ for the thin film over $c=-0.4$ for the intermediate film to $c=-0.2$ for the thickest film investigated. This behavior can be interpreted as a gradual transition from a discontinuous island structure with non-Drude conductivity to more homogeneous films with Drude-like conductivities as more clusters are deposited. We would like to point out that this observation of a continuously changing persistence of velocity parameter c is very similar to the behavior near the metal-insulator percolation transition in evaporated gold films,[3] though it occurs not nearly as abrupt.

For our set of samples, the best antireflection performance was displayed by film 2 which, shows a very broadband, nearly perfect reflection suppression. Since, however, for the cluster films the parameter c is thickness dependent, the performance degrades if thicker films are required, e.g., for substrates with larger refractive indices. Nevertheless, in spite of this deficiency, these films still should offer a better broadband performance than bulk metallic coatings since c is always <0.

V. FINITE-DIFFERENCE TIME-DOMAIN SIMULATION

Figure 8 displays the effect of the gold film's thickness on its reflectivity. Only a film with exactly the right thickness can optimally suppress reflections at the interface silicon-air, with films thinner and thicker than this optimal thickness d_{opt} leading to increased reflection without and with a reversal of polarity, respectively. In order to assess the potential of an antireflection coating by using nanostructured gold films, the processes close to the optimal thickness must be investigated. Unfortunately, the preparation of such gold films is tedious and exact control over the film thickness is difficult to attain. By using the results of the measurements described earlier in this paper, however, computer simulations could be run, giving insight into the behavior of the internal reflection at films near the optimal thickness.

Due to the broad spectra of terahertz pulses, the finite-difference time-domain (FDTD) method was chosen over harmonic approaches, which are limited to simulating monochromatic radiation. The FDTD method represents a discrete form of the time-dependent Maxwell equations, in which derivatives are replaced with difference quotients.[27] Given initial field distributions $\vec{E}(\vec{x}_i)$, $\vec{H}(\vec{x}_j)$ on a discrete spatial grid, the FDTD method can be used to calculate their time development. The discretization grid must be chosen to be large enough to store the simulated geometry and wave forms as well as fine enough to resolve even the smallest occurring field or material structures. As the large scale difference between wavelength ($\lambda \sim 300\ \mu$m) and film thickness ($d \sim 8$ nm) in our experiment leads to extremely large grids and, consequently, disproportionally high computational

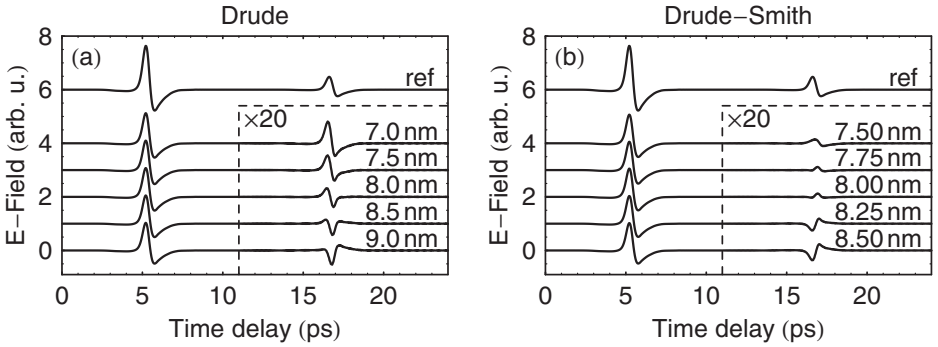

FIG. 10. FDTD simulations of a system equivalent to the described experimental setup with films near the optimal thickness. The curves compare the behavior of uncoated (ref) and gold-coated silicon substrates. Simulations were performed by using both the (a) Drude and (b) Drude–Smith models to simulate the gold. The internal reflections (inside the dashed box) are small and thus shown magnified 20 times.

costs when using a uniform discretization grid, a subgridding scheme especially conceived for a very high local grid refinement was implemented.[28] This scheme intends for grid refinement by a large factor to be limited to a fraction of a grid cell, providing the resolution necessary to resolve the very thin gold film while keeping computational costs small. The option to chose an arbitrary refinement factor $N \in \mathbb{R}$ allows to vary the film thickness around a given value in steps much smaller than the grid spacing: In our simulations, the gold film was a fixed four grid steps thick, while varying the grid spacing around 2 nm in small steps enabled a very fine control of the film thickness around 8 nm.

To be able to compare the two approaches, simulations were run by using both the Drude and the Drude–Smith model to describe the gold. As all calculations of the FDTD method are performed in the time domain, simulating frequency-dependent behavior is not straightforward. By using methods from digital signal processing, the frequency-dependent conductivity $\sigma(\omega)$ of the gold could be implemented into the simulation as a convolution in the time domain by using a process known as an infinite impulse response filter, which can be analytically calculated from both the Drude and Drude–Smith models.[29,30]

Figure 10 shows FDTD simulations of a system equivalent to the described experimental setup. In all cases, the film thickness was chosen to be very close to the optimal thickness; hence, the amplitudes of the internal reflections, displayed inside the dashed boxes, are very small and thus shown magnified 20 times. In both Figs. 10(a) and 10(b), one can see how increasing the film thickness results in a minimum in the reflected amplitude, followed by a reversal of polarity of the reflected pulse as the optimal thickness is exceeded. However, the minimum amplitude in the simulations using the Drude model, at 8.5 nm, is about five times larger than the smallest reflected pulse in the simulations implementing the Drude–Smith model, at 7.75 nm. This is consistent with the expected reflection coefficients shown in Fig. 5 and demonstrates how the change in conductivity caused by the structure of the gold film, modeled by the Drude–Smith formalism, can result in a significantly improved impedance matching at the silicon-air transition.

VI. CONCLUSION

This study demonstrates that nanostructured gold films can serve as broadband impedance-matching coatings for substrates and optics in the terahertz frequency range. We show in theory and experiment that the internally reflected electric field amplitude of a broadband terahertz pulse in a silicon substrate can be suppressed to below 1% of that without coating, which is at least a factor of 5 better than the best suppression achievable with bulk gold layers. This superior performance is due to the non-Drude behavior of the nanostructured films, which can be described well by the Drude–Smith model, a generalization that incorporates carrier localization through enhanced backscattering. As a consequence, the films in this study exhibit nearly frequency-independent optical properties over the entire spectral range covered by our experiment. This allows us to perfectly match wave impedances across the interface between different nondispersive substrates or between a substrate and air over a broad bandwidth by choosing the optimal film thickness. By using FDTD simulations, the thickness-dependent reflection behavior at the silicon-gold-air interface was investigated with subnanometer precision. Randomly nanostructured gold films as impedance-matching coatings are particularly useful for applications where even weak internal reflections in the optical components would obscure the data and, therefore, cannot be tolerated, e.g., in high-precision spectroscopy.

ACKNOWLEDGMENTS

The authors are grateful to Bernd von Issendorff for fruitful discussion and for providing the cluster deposition facilities and to Chunrong Yin and Mischa Schmidt for the preparation of the gold samples. They also wish to acknowledge Yi Thomann from the Freiburg Materials Research Center for characterizing the films by atomic force microscopy.

[1] J. Kröll, J. Darmo, and K. Unterrainer, Opt. Express **15**, 6552 (2007).
[2] J. Kröll, J. Darmo, and K. Unterrainer, Electron. Lett. **40**, 763 (2004).
[3] M. Walther, D. G. Cooke, C. Sherstan, M. Hajar, M. R. Freeman, and F. A. Hegmann, Phys. Rev. B **76**, 125408 (2007).
[4] Y. Yagil, P. Gadenne, C. Julien, and G. Deutscher, Phys. Rev. B **46**, 2503 (1992).
[5] B. Gompf, J. Beister, T. Brandt, J. Pflaum, and M. Dressel, Opt. Lett. **32**, 1578 (2007).
[6] H. Miyake, S. Ye, and M. Osawa, Electrochem. Commun. **4**, 973 (2002).
[7] H. Haberland, M. Karrais, M. Mall, and Y. Thurner, J. Vac. Sci. Technol. A **10**, 3266 (1992).
[8] O. Rattunde, M. Moseler, A. Häfele, J. Kraft, D. Rieser, and H. Haberland, J. Appl. Phys. **90**, 3226 (2001).
[9] P. Uhd Jepsen, B. M. Fischer, A. Thoman, H. Helm, J. Y. Suh, R. Lopez, and R. F. Haglund, Jr., Phys. Rev. B **74**, 205103 (2006).
[10] M. van Exter, Ch. Fattinger, and D. Grischkowsky, Opt. Lett. **14**, 1128 (1989).
[11] O. S. Heavens, *Optical Properties of Thin Solid Films* (Dover, New York, 1991).
[12] F. Gao, G. L. Carr, C. D. Porter, D. B. Tanner, G. P. Williams, C. J. Hirschmugl, B. Dutta, X. D. Wu, and S. Etemad, Phys. Rev. B **54**, 700 (1996).
[13] M. Dressel and G. Grüner, *Electrodynamics of Solids* (Cambridge University Press, Cambridge, 2002).
[14] M. Born and E. Wolf, *Principles of Optics*, 7th ed. (Cambridge University Press, Cambridge, 1999).
[15] D. G. Cooke, A. N. MacDonald, A. Hryciw, J. Wang, Q. Li, A. Meldrum, and F. A. Hegmann, Phys. Rev. B **73**, 193311 (2006).
[16] M. Tinkham, Phys. Rev. **104**, 845 (1956).
[17] M. A. Ordal, L. L. Long, R. J. Bell, S. E. Bell, R. R. Bell, R. W. Alexander, Jr., and C. A. Ward, Appl. Opt. **22**, 1099 (1983).
[18] J. C. Maxwell-Garnett, Philos. Trans. R. Soc. London, Ser. A **205**, 237 (1906).
[19] D. A. G. Bruggeman, Ann. Phys. (Paris) **24**, 636 (1935).
[20] Y. Yagil, M. Yosefin, D. J. Bergman, G. Deutscher, and P. Gadenne, Phys. Rev. B **43**, 11342 (1991).
[21] J. P. Clerc, G. Giraud, J. M. Laugier, and J. M. Luck, Adv. Phys. **39**, 191 (1990).
[22] J. B. Baxter and C. A. Schmuttenmaer, J. Phys. Chem. B **110**, 25229 (2006).
[23] M. C. Beard, G. M. Turner, J. E. Murphy, O. I. Micic, M. C. Hanna, A. J. Nozik, and C. A. Schmuttenmaer, Nano Lett. **3**, 1695 (2003).
[24] E. Hendry, M. Koeberg, B. O'Regan, and M. Bonn, Nano Lett. **6**, 755 (2006).
[25] G. M. Turner, M. C. Beard, and C. A. Schmuttenmaer, J. Phys. Chem. B **106**, 11716 (2002).
[26] N. V. Smith, Phys. Rev. B **64**, 155106 (2001).
[27] K. S. Yee, IEEE Trans. Antennas Propag. **AP-14**, 302 (1966).
[28] A. Kern and M. Walther, J. Opt. Soc. Am. B **25**, 279 (2008).
[29] W. Tong, Z. Wenjun, and L. Weiliang, Proceedings of International Conference on Computational Electromagnetics and Its Applications (ICCEA, 1999) (IEEE, 1999), pp. 48–51.
[30] D. M. Sullivan, IEEE Trans. Antennas Propag. **AP-40**, 1223 (1992).